ORIGINAL PAPER

Prediction of EDMed micro-hole quality characteristics using hybrid bio-inspired machine learning-based predictive approaches

Thella Babu Rao[1]

Abstract

Micro-meter range material removal is an indispensable requirement in today's industrial scenario for precision components manufacturing in the medical, optical, automobile, and aerospace industries. The dimensional accuracy and material removal rate are highly correlated and important drilled micro-hole characteristics in the micro-electric discharge machining (μEDM) process. In this investigation, predictive models based on bio-inspired intelligent hybrid machine learning algorithms are proposed for machining micro-holes with accurate dimensions on Inconel 718 superalloy by μEDM process. The recast layer thickness and radial overcut are considered as the produced hole dimensional quality features and the material removal rate as the production rate indicator. The proposed predictive models are based on the integration of adaptive neuro-fuzzy inference system (ANFIS) with genetic algorithm (ANFIS-GA) and particle swarm optimization algorithm (ANFIS-PSO). Here, the precision of the ANFIS model was improved by optimizing its algorithmic parameters with the application of GA and PSO individually. Experimentally measured machining response data was used for training, testing, and validation of the models. The performance of the proposed predictive models was assessed based on the statistical parameters. The predicted training and testing values for the responses with regression, ANN, ANFIS, ANFIS-GA, and ANFIS-PSO models were in good agreement with their corresponding experimentally measured values. The estimated values of statistical parameters representing the μEDM responses suggest that the ANFIS-PSO model predicts more accurately as compared with other models. A comparative analysis of the predictability of the proposed models with respect to the experimental results is also presented for confirming the reliability of the ANFIS-PSO model for accurate perdition of the μEDM process.

Keywords μ-EDM · Recast layer thickness · Radial overcut · Material removal rate · ANN · ANFIS · ANFIS-GA · ANFIS-PSO

1 Introduction

Machining of micron-size holes in difficult-to-cut materials remains a complex task though the present manufacturing industries are equipped with advanced machining and tooling technologies due to the material's mechanical properties and size of the hole. Inconel 718 (Ni718) superalloy is an important material being used today for manufacturing a wide range of aero-engine, rocket, gas turbine, and submarine components that are functioning between 450 and 700 °C temperatures [1]. Superior thermal and corrosion resistance and high yield and ultimate strength, high hot hardness with

Ni718 alloy are attractive properties for a widespread applications in the electronics, chemical, and marine industries [2, 3]. However, the properties such as poor thermal conductivity and work hardening tendency of Ni718 alloy made it classify as the difficult-to-machine material [4] using traditional machining practices. Since, there is no mechanical contact in nontraditional machining approaches between the workpiece and tool, the chip formation in metal removal is independent of the workpiece hardness [5]. Hence these approaches have been proved as efficient for machine materials irrespective of their hardness [6].

Electro-discharge machining (EDM) is a popularly commercialized nontraditional machining process in manufacturing industries for machining precision components that require a high degree of surface quality and dimensional accuracy. Due to high tool wear and chatter, machining of

✉ Thella Babu Rao
   thellababurao@nitandhra.ac.in

1 Department of Mechanical Engineering, National Institute of
   Technology Andhra Pradesh, Tadepalligudem, West Godavari
   District, Andhra Pradesh 534102, India

micro-features on difficult-to-cut and heat resistance materials such as Inconel alloys to achieve the required surface quality and drill accuracy through conventional drilling process become very difficult and involved with a huge expenses [7]. Micro-EDM (μEDM) as a version of the EDM process has been identified as an appropriate nonconventional machining process for machining micron-size holes on Ni718 alloy within the limits of the desired tolerance [8]. Also, μEDM allows to generate micro-textures and devices for a wide range of industrial, aeronautical, electronics and the biomedical applications. In the μ-EDM process, due to the generation of high-intensity heat by the rapid recurring electric sparks [9], a small portion of the material in the form of debris is removed from the workpiece by melting and evaporation. The debris formed by melting are flushed from the workpiece electrode interface by the continuous supply of dielectric fluid. Despite of several advantages with the μEDM process, radial overcut, tool wear rate, and material removal rate are pointed out as its limitations. Hence, several research investigations have been reported on the fundamental understanding of various process characteristics for better control of its performance towards the machining efficiency improvement. Type, size and shape of the electrode, electrode feed rate, polarity, current density, gap voltage, pulse-on time, pulse-off time, duty cycle, type of dielectric and its pressure are some of the frequently considered process control variables of μEDM. While the material removal rate (MRR), tool wear rate (TWR), surface roughness, diameter radial deviation, hole taper angle, recast layer, and radial overcut are the μEDM performance indicating characteristics. Higher feed rates increase the MRR as it accelerates the sparking rate at the workpiece-tool gap, but it also increases the formation of the recast layer on the machined surface which reduces the surface quality [10]. MRR is increased by increasing the peak current as it increases the material melting rate by increasing the discharge energy. Increasing the peak current simultaneously increases the TWR [11] which is an adversely effect the machine hole dimensional accuracy. The use of negative polarity increases the density of electrons reaching the workpiece which simultaneously improve the MRR and reduce the TWR compared to positive polarity [12, 13]. De-ionized water gives better MRR and TWR than kerosene as dielectric [14]. The larger electrode diameter increases the TWR due to the continuously changing discharge conditions and higher discharge frequency [15].

The occurrence of secondary discharge at the electrode-drilled home gap due to the movement of debris generate progressively tapered hole [16]. Lim et al. [17] investigated the influence of voltage, gap control algorithm, and capacitance and resistance values in μEDM on TWR, MRR, and the stability of the machining. Ay et al. [18] noted better micro hole quality at low pulse duration and low discharge current. The tool orbital actuation reduces the tool wear and

improves the machined surface quality by accelerating the electrode flushing [19]. Natarajan et al. [20] observed better micro hole topographical conditions at lower values of pulse-on time and discharge current. A better surface finish in μEDM can be obtained by sacrificing the MRR while the acceleration of MRR results in higher surface roughness and TWR. Therefore, Muhammad et al. [12] proposed an ideal set of process parameters to deliver better μEDM performance for machining WC–Co. Rao et al. [21] derived an optimal processing conditions for μEDM Ni718 alloy based on the experimental observations pertaining to the MRR, TWR, and recast layer by the conduction of design of experimentation and gray relational analysis integrated Taguchi's statistical approach.

Likewise, several authors have performed experimental studies to understand the significance of many adjustable process parameters of μEDM on its response characteristics. However, the knowledge of these investigations may not be enough to evaluate the μEDM process performance for real-time machining on the shop floor. In general, the selection of μEDM process parameters is done by using either the data manual provided by the machine tool manufacturer and/or the machine tool operators' experience. But such criteria neither guarantee the desired drilled hole dimensional characteristics nor the surface quality due to the presence of highly conflicted process responses. Hence, the choice of a suitable set of machining conditions meeting the desired quality characteristics become a complicated task. Such circumstances made selection of optimal μEDM processing conditions quite essential through a reliable approach to enhance the machining performance. But considering the confliction among μEDM process responses for a large number of process control parameters, optimization of any one response alone cannot represent the complete performance of the process in real practice. Dealing with such conflicted responses required a method of simultaneous optimization of multiple responses. Hence, statistical and intelligent modeling and optimization of the process responses gained more attention for simultaneous optimization of multiple conflicted responses to enhance the machining process efficiency [5].

Deepak et al. [10] considered the process parameters: voltage, electrode rotation speed, and feed rate of μEDM to optimize its responses such as MRR, overcut (OC), and taper angle using the genetic algorithm proposed sum of weighted objectives technique for machining Ni718 alloy. Somashekhar et al. [22] shown artificial neural network (ANN) model as effective for MRR prediction in μEDM with the develop a parametric regression model. Anthony et al. [23] employed the ANN model to obtain optimal tool profiles instantaneously and their results showed considerably very little deviation from the experimentally measured results. The prediction accuracies of ANN and adaptive neuro-fuzzy

interference system (ANFIS) models for μEDM process performance characteristics were compared by Suganthi et al. [24] and noted superior predictability with the ANFIS model. Recently, by Ashish et al. [25] implemented response surface methodology (RSM) to predict the significance of various EDM process parameters on MRR, SR, and TWR and ANFIS to derive the optimal processing conditions for machining Inconel alloy. The results of their validation experiments are observed with a good agreement with the predicted results. Pathak et al. [26] presented the studies on the circularity and surface roughness against various control parameters of powder-EDM process for machining Inconel 718 alloy and determined their optimal values by implementing fuzzy logic and ANFIS models. They reported better prediction with ANFIS model compared with the fuzzy model. Singh et al. [27] integrated gray relational analysis (GRA) with ANFIS method to derive the optimal EDM conditions for machining WC alloy. In gas-assisted μEDM of D3 die-steel, Nishant et al. [28] employed an integrated neuro-fuzzy model and GA optimization approach to predict and analyze the responses such as MRR and surface roughness. GA has been used to improve the model architecture of the ANFIS as well as to determine the optimal set of machining conditions. Compared with the results of ANN and ANFIS models, ANFIS integrated GA has shown better performance for the prediction of the machining conditions. To adopt the dynamic realistic non-linear relationships among the response, and to treat all the responses based on their degree of significance among them in statistical analysis, Ishwar et al. [29] used principal component analysis (PCA) to normalize the response data of MRR, TWR, and OC of μEDM process performed on a silver plate and the normalized data was fed as input to ANFIS model for process optimization. Lingxuan et al. [30] integrated multi-objective GA with supporting vector machine (SVM) prediction model for prediction and optimization of TWR and machining time in μEDM process. Assarzadeh et al. [31] employed ANN model for prediction and augmented Lagrange multiplier algorithm for optimization of μEDM conditions.

Owing to the above-conferred investigations on the implementation of various predictive modeling and parametric optimization approaches for improvement of the μEDM process, it has been noted that, a handful number of investigations have been used ANN modeling technique. This is due to the reason that, ANN is a flexible process modeling tool inspired by the biological nervous system [32] having the capability of mapping a nonlinear mathematical relationship between several process input variables and a response [31]. However, the application of the ANN modeling technique is limited by the problem of overfitting the response values because it follows the "black-box models" trained by sampling data of input variables and output response rather than the machining process mechanism. Moreover, a large number of data samples should be provided train the network as a well-trained ANN model. Determination of a reliable network architecture is also a complex task and is depending on experiences. Therefore, Saffaran et al. [33] optimized the network architecture with the help of the PSO (particle swarm optimization) algorithm, and the performance of the determined architecture was verified by SA (simulated annealing) algorithm. Recently, the ANFIS modeling technique has been proved as one of the potential predictive modeling techniques for complex nonlinear machining processes. ANFIS evolved with the integration of two popular soft-computing techniques of ANN and fuzzy logic. ANN in ANFIS has the capability of self-understanding the relation between the input and response data while fuzzy logic holds the capability of dealing with imprecision and uncertainty present with the data using if–then fuzzy rules [34].

Based on the available literature, efficient approaches are vital for exact prediction of the precise machining processes to minimize the model's uncertainty. The stat-of-affairs result in the hybridization of the suggested predictive models in the literature for the development of efficient predictive models for the μEDM process is motive of this investigation. Nevertheless, being implemented μEDM for manufacturing a wide range of components in many fields, the literature review shows that no research work is published on the comparative analysis of the reliability of ANN, ANFIS, ANFIS-GA, and ANFIS-PSO algorithms for prediction of μEDM responses.

2 Research significance and novelty

Since, micro-meter range material removal is an indispensable requirement in today's industrial scenario for manufacturing precision components for medical, optical, automobile, and aerospace industries. A high degree of dimensional accuracy and surface quality of the machined micro-holes are the desired functional performance characteristics, and the material removal rate reflects the production rate of the components in μEDM process. However, the dimensional accuracy and material removal rate are highly correlated and important drilled micro-hole characteristics in processing micro-features by μEDM process. While producing quality micro-features by μEDM is involved with the control of a large number of process parameters. Conduction of the trail machining experiments for identification of set optimal machining conditions is relatively time-consuming and costly. Therefore, efficient predictive and optimization approaches are vital for a more precise prediction of the machining conditions to enhance the machining efficiency. Owing to the proposed predictive and optimization approaches in the literature aiming with various machining process, the selection of a reliable approach is still ambiguous

Fig. 1 ANFIS architecture based on Sugeno fuzzy model
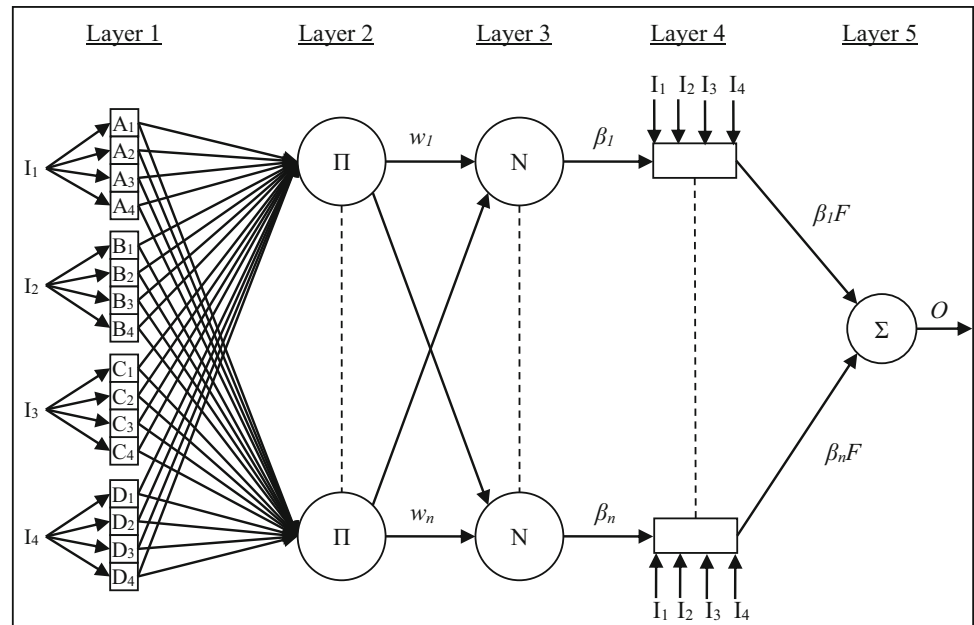
as every approach may not efficiently predict every machining process. Recently, the application of machining learning algorithms has been popularly used for prediction of various machining process. However, the prediction efficiency of a machine learning algorithm in turn need an appropriate selection of the algorithm-centric control variable. While still there are no stipulated guidelines or constructive formulations to determine the necessary number of MFs in the literature. Hence this investigation presented the evaluation of a reliable machine learning algorithms and allied intelligent hybrid approaches for μEDM performance prediction and experimentally proved for their shop-floor implementation. Also, the results of this investigation explained and compared the precision of ANFIS-PSO, ANFIS-GA, ANFIS, ANN, and regression models for predicting the μEDM performance characteristics. This kind of investigation has been not reported yet in the literature in application to the μEDM process performance evaluation in terms of the chosen microhole characteristics such as recast layer thickness, diametral deviation, and MRR.

3 Model development

3.1 Adaptive network-based fuzzy inference system (ANFIS)

A Neuro-fuzzy system (NFS) was proposed by Jang in 1983 based on the integration of ANN and Fuzzy-rule based interface system [34, 35]. This interface system allows the flexible estimation with the capability of exploring interpretable Takagi–Sugeno type fuzzy If–then rules. ANFIS

correlates the output and input data by using an integrated learning approach for obtaining the optimal spreading of different membership functions (MF's). The rationalization of MF's in ANFIS is done in two ways such as back and hybrid propagation. ANFIS architecture is designed with 5 layers integration and each layer is defined by a node function as shown in Fig. 1: "input fuzzification as layer 1", "fuzzy set database creation as layer 2", "fuzzy rule base structure as layer 3", "decision-making as layer 4", and "output defuzzification as Layer 5" [36, 37].

The five layers of the ANFIS model are described as:

Layer 1 The set of input values is converted into a set of if–then fuzzy rules by the selection of appropriate MFs for each input set. For instance, the general bell-shaped membership function (gbellmf's) of the adaptive node is defined as:

Membership function of the first parameter:

$$\mu A_i(I_1) = \frac{1}{1 + \left[\left(\frac{I_1 - c_i}{a_i}\right)^2\right] \times b_i} \tag{1}$$

Membership function of the second parameter:

$$\mu B_i(I_2) = \frac{1}{1 + \left[\left(\frac{I_2 - c_i}{a_i}\right)^2\right] \times b_i} \tag{2}$$

Membership function of the third parameter:

$$\mu C_i(I_3) = \frac{1}{1 + \left[\left(\frac{I_3 - c_i}{a_i}\right)^2\right] \times b_i} \tag{3}$$

Membership function of the fourth parameter:

$$\mu D_i(I_4) = \frac{1}{1 + \left[\left(\frac{I_4 - c_i}{a_i}\right)^2\right] \times b_i} \tag{4}$$

Here, μA_i, μB_i, μC_i and μD_i are the MFs of the input variables I_1, I_2, I_3 and I_4 respectively. The parameter sets a_i, b_i, and c_i, for which the fuzzy membership values vary between 0 and 1. The membership functions change according to the varying values of the parameters and are not constant. The parameters in this layer are called "principle parameters".

Layer 2 The output signal in this layer is calculated by the multiplication of the input signal with the fuzzy operator as:

$$w_i = \mu A_i(I_1) \times \mu B_i(I_2) \times \mu C_i(I_3) \times \mu D_i(I_4); \, i$$
$$= 1, \, 2, \, 3, \, 4, \, \ldots \tag{5}$$

Here, w_i signifies the "strength" of the fuzzy rule setup. The nodes in this layer are termed "rule nodes" and are fixed.

Layer 3 In this layer, the normalized node strength for every neuron is calculated as:

$$N_i = \frac{w_i}{\sum_i w_i}; \, i = 1, \, 2, \, 3, \, 4, \, \ldots. \tag{6}$$

Layer 4 Here the fuzzy quantity is de-fuzzified. Every node is an adaptive node holding a node function. The combined membership functions and fuzzy rules are represented as:

$$N_i \times F_i = N_i \cdot (p_i \cdot (I_1) + q_i \cdot (I_2) + r_i \cdot (I_3) + s_i \cdot (I_4)); \, i$$
$$= 1, \, 2, \, 3, \, \ldots \tag{7}$$

where, p_i, q_i, r_i and s_i are the parameter set at each node, N_i is the normalized node strength and F_i is the fuzzy rule.

Layer 5 This layer gives the overall output of the system by summation of all incoming signals as:

$$Overall \ output = \sum_i N_i \times F_i = \frac{\sum_i N_i \times F_i}{\sum_i N_i} \tag{8}$$

3.2 Integrated ANFIS (ANFIS-GA & ANFIS-PSO) model

The ANFIS modelling variables are generally adjusted by steep descend error or least square error methods. However, these two optimization approaches cannot result in the global optimal solution and hence the solution may be trapped in local optima. Also, the algorithmic parameters of ANFIS such as the number of neurons, hidden layers, initial weights, membership functions, etc. are derived by the trial–error approach. To conquer with such limitations, the
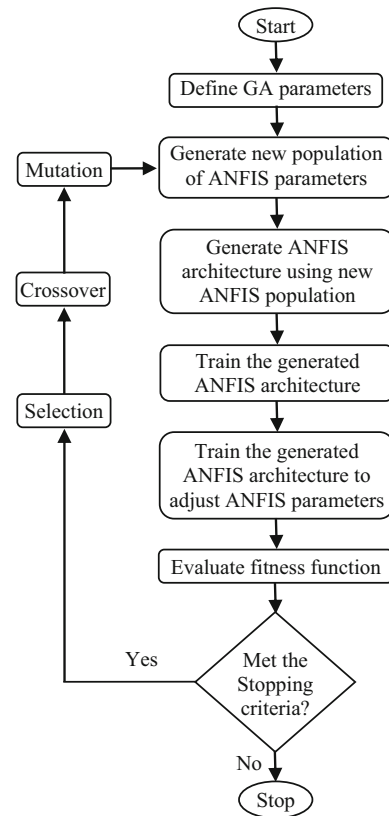

Fig. 2 The scheme of ANFIS-GA hybrid algorithm

researchers proposed an integrated approach of ANFIS-GA to enhance the predictability of the ANFIS model to find the global optimal value. In the ANFIS-GA approach, the important parameters such as population size, Maximum number of generations, mutation percentage, crossover percentage, selection, mutation rate, number of fuzzy rules, type and number of membership functions are algorithmic parameter inputs of simulation to estimate the optimal fitness function. While as per the discussions reported in the literature, the most significant ANFIS-PSO algorithmic parameters are the maximum number of iterations, the maximum number of particles, initial inertia weight, inertia weight damping ratio, personal learning coefficient, global learning coefficient, number of fuzzy rules. The main intention of GA and PSO algorithms integration with ANFIS is to adjust such ANN and fuzzy algorithmic parameters to minimize the specified objective function. ANFIS integrated GA approach has been popularly used for solving a variety of engineering problems [38–40].

Similarly, the PSO integrated ANFIS model has been also implemented to solve many manufacturing problems in recent investigations [37, 41]. The flowchart of ANFIS-GA integrated algorithm and ANFIS-PSO integrated algorithm are respectively presented in Figs. 2 and 3.
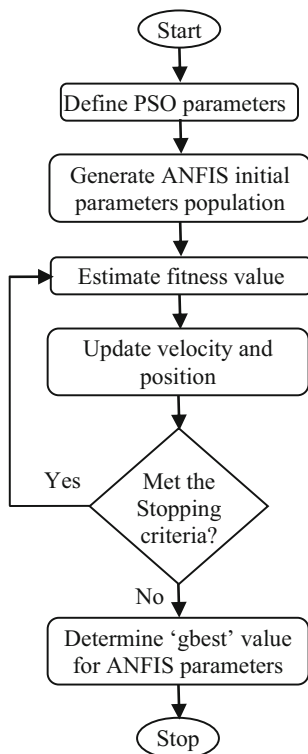
Fig. 3 The scheme of ANFIS-PSO hybrid algorithm

Fig. 4 The chemical composition of as-received Ni718 alloy workpiece determined by EDS analysis

4 Experimental details and measurement of μ-EDM responses

The micro-through holes by μEDM process for the present investigation have been processed on a 3 mm thick aerospace Ni718 superalloy plate by using a 3 axis CNC EDM machine (model: ZNC S430, Acro Machinery & Electric Co., Ltd, Taiwan). The commercially available cylindrical copper electrode of 800 μm diameter was used as the tool electrode. TOTAL EDM3 oil was used as the dielectric fluid and supplied to the machining zone continuously at a flushing pressure of 0.4 kg/cm^2 to wash away the formed debris

molten at the workpiece-tool gap. The details of the experimental parameters and other machining conditions which are used to perform μEDM holes are given in Table 1. While the chemical composition of the as received workpiece determined by EDS analysis is presented in Fig. 4. The experimental design consists of a total of 36 experimental runs based on the Taguchi's orthogonal mixed-level design and 3 repetitive and unnecessary tests were not considered for the experimentation [5]. The machine-dependent permissible ranges of μEDM input parameters such as Pulse on time, Current, Voltage and Duty cycle were determined by conducting the pilot experimental runs prior to the conduction of actual machining experiments. Each experiment in the design matrix was conducted for a depth of 3 mm.

Production rate, surface quality, and dimensional accuracy are the most important μEDM process performance evaluation parameters concerned with the quality cut. Therefore, the
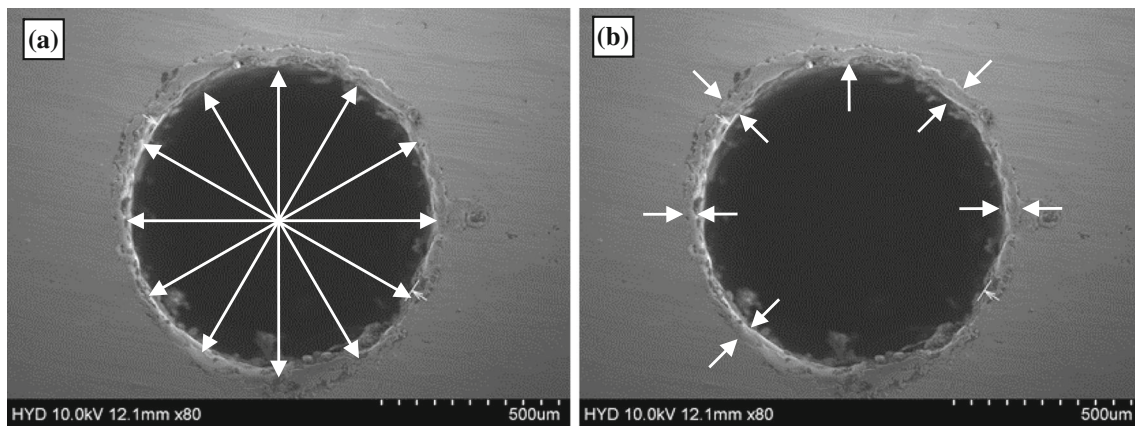
Table 1 Details of the experimental parameters

S. No	Variable factors	Units	Notation	Level 1	Level 2	Level 3
1	Pulse on time	μs	x_1	60	80	100
2	Current	Amp	x_2	3	6	9
3	Voltage	V	x_3	50	60	70
4	Duty cycle	%	x_4	70	80	90
Dielectric used: EDM commercial grade oil						
Dielectric flushing: Side flushing with pressure						
Workpiece material: Inconel 718 alloy						
Electrode material: Electrolytic pure copper						
Electrode polarity: Possitive						
Workpiece polarity: Negative						

Fig. 5 Measurement of μEDMed **a** hole diameter and **b** recast layer thickness

machining experiments in this study are conducted to measure the material removal rate (MRR), recast layer thickness (RLT), and radial overcut (ROC) as μEDM process responses to evaluate them and predict the process performance. MRR represents the production rate of μEDMed components. The formation of the recast layer on the machined surface alters the metallurgical properties and hardness of surface and sub-surface regions which predominantly influence the corrosion and fatigue characteristics of the machined part. Therefore, the RLT represents the quality of μEDMed hole surface integrity. While the ROC represents the dimensional accuracy of the machined hole. MRR (in mg/min) was estimated as the difference in weight of the workpiece before and after making drill per machining time. A high-precision digital weighing machine was used for accurately measuring the weights of the workpiece samples before and after the conduction of machining experiment. The recast layer in the radial direction and machined micro-hole diameter was measured on scanning electron micrographs using an image analyzer software. A total of six readings were taken on each machined hole to estimate recast layer thickness and machined hole diameter individually and their average was considered as the final response values respectively. ROC was estimated as the difference between the initial diameter of the tool electrode and the diameter of the machined hole measured. The readings of RLT and ROC are taken on the top surface of the machined micro-hole. In Fig. 5, the measurement of RLT and ROC on machined micro-hole SEM images is shown. The measured experiment results are reported in Table 2.

5 Results and discussion

Initially, the adequacy of the experimentally measured μEDM process response values was evaluated by ANOVA. Table 3 present the ANOVA of the process responses. The p-value less than 0.05 in Table 3 estimated using ANOVA represent that the postulated models and selected variables are significant to predict the process responses statistically at a confidence level of 95% [42]. Accordingly, based on the results presented in Table 3, all the response models postulated for this investigation are statistically significant. The multiple regression coefficient values (R^2 values) in Table 3 for the responses MRR, RLT, and ROC are 0.9898, 0.9992, and 0.9947 respectively. These values indicate that the respective model of MRR, RLT, and ROC can estimate their corresponding measured response with 98.98%, 99.92%, and 99.47% accuracy.

5.1 Prediction of μEDM responses by ANN

ANN procedure map the process response between the input process control variables to solve complex problems [43]. The ANN consists of interconnected constituent neural components that are capable learn, discrete, and prepare the data for prediction [44]. The ANN architecture was constructed with input, hidden, and output layers. The neural components in ANN architecture can mimic a human in learning from the provided social event data for prediction. The application of ANN in the recent past investigation has been considered very significant for modeling and prediction of several machining process quality characteristics. In consideration of its computational capabilities, in this investigation, ANN has been used for modeling and prediction of μEDM performance characteristics. The number of neurons in the input layer represents the chosen process control variables and the output layer neurons are the μEDM responses. While the number of hidden layers and the number of neurons in each hidden layer must be derived through trial and error. To construct a perfect ANN architecture for the present problem, MATLAB programming was used. The input layer consists of the chosen four μEDM variables linked to the concealed

Table 2 Experimental design and measured response values

Exp. No	Pulse-on time (μs)	Current (Amp)	Voltage (V)	Duty cycle (%)	MRR (mg/min)	RLT (μm)	ROC (μm)
1	60	3	50	70	0.354	48.673	962
2	80	6	60	80	0.525	41.905	965
3	100	9	70	90	0.942	55.311	1025
4	80	9	50	70	0.556	64.475	859
5	100	3	60	80	0.542	43.965	954
6	60	6	70	90	0.541	38.213	990
7	100	6	50	70	0.529	60.828	1000
8	60	9	60	80	0.646	48.708	935
9	80	3	70	90	0.425	35.117	867
10	100	3	50	80	0.479	46.864	987
11	60	6	60	90	0.496	43.637	1005
12	80	9	70	70	0.817	55.433	999
13	100	6	50	80	0.521	50.917	984
14	60	9	60	90	0.728	52.506	1003
15	80	3	70	70	0.432	42.538	949
16	60	9	50	80	0.488	51.366	877
17	80	3	60	90	0.454	41.661	931
18	100	6	70	70	0.676	52.545	1025
19	80	9	50	80	0.559	53.87	884
20	100	3	60	90	0.565	48.151	938
21	60	6	70	70	0.458	46.023	987
22	80	3	50	90	0.383	44.532	982
23	100	6	60	70	0.652	58.023	1018
24	60	9	70	80	0.743	43.378	980
25	80	6	50	90	0.452	48.742	999
26	100	9	60	70	0.884	66.58	986
27	60	3	70	80	0.365	30.171	890
28	100	9	50	90	0.823	63.808	970
29	60	3	60	70	0.437	46.029	955
30	80	6	70	80	0.556	36.454	965
31	60	6	50	90	0.355	46.388	1015
32	80	9	60	70	0.746	60.790	935
33	100	3	70	80	0.486	38.393	909

neuron layer, and the output layers of μEDM responses considered in this work are connected to the shrouded layer. From several trials execution of the program, the determined ANN architecture model for the responses is shown in Fig. 6.

Each hidden layer in the developed model comprises 19 neurons, four input, and one output neuron. Levenberg–Marquardt feed-forward with back-propagation learning (FFBP) architecture was used for the training of the ANN system for fast and intensive learning [44, 45] and to predict the response values. The estimated value of mean square relative error (MSRE) between the experimental data and the estimated output response values is the performance

measure of the constructed FFBP network. MSRE is the average square between the network output values and experimental targeted values. The zero value of MSRE represents the zero error between the targeted values and the predicted values and therefore, a lower value of MSRE is preferred. The MSRE between the experimental and ANN predicted response values corresponding to MRR, RLT, and ROC are 0.0077, 0.0211, and 0.0012 respectively. On the other hand, the regression value (R-value) is another measure of network efficiency. R values estimate the correlation between the targeted (experimentally measured) values and predicted output values by the network. An R-value of 1

Table 3 Significance of μEDMcontrol variables and fit statistics of response models

μEDM control variables	p-value		
	MRR	RLT	ROC
Model	< 0.0001	< 0.0001	< 0.0001
x_1	< 0.0001	< 0.0001	< 0.0001
x_2	< 0.0001	< 0.0001	< 0.0001
x_3	< 0.0001	< 0.0001	< 0.0001
x_4	0.0079	< 0.0001	< 0.0001
x_1x_2	0.0086	0.0757	0.0304
x_1x_3	0.0242	0.1287	0.0039
x_1x_4	0.4047	0.0012	< 0.0001
x_2x_3	< 0.0001	0.7082	< 0.0001
$x_2 x_4$	0.0066	0.9017	< 0.0001
$x_3 x_4$	0.2978	0.2364	< 0.0001
x_1^2	0.0155	< 0.0001	< 0.0001
x_2^2	< 0.0001	< 0.0001	< 0.0001
x_3^2	< 0.0001	< 0.0001	0.0022
x_4^2	0.0099	< 0.0001	< 0.0001
Fit Statistics			
R^2	0.9898	0.9992	0.9947
Adj-R^2	0.9819	0.9987	0.9906
Pred-R^2	0.9230	0.9969	0.9793

represents accurate predictability of the response values by developed network, whereas, the random relationship between the predictive model and targeted values for R value is zero. The simulated correlation coefficients (R values) for this investigation corresponding to the chosen μEDM responses: MRR, RLT, and ROC are 0.9914, 0.9105 and 0.9481 respectively as shown in Fig. 7.

The regression coefficient (R^2) values estimated for the chosen μEDM responses: MRR, RLT, and ROC are closer to 1 is the indication for that the constructed network mapped the chosen μEDM inputs to its outputs closely and can be used for prediction precisely. Accordingly, the prediction capability of the constructed FFBP network can be evaluated and determined its scope applicability for a machining process prediction [46]. In ANN predictability for the experimental data collected in this investigation is presented in
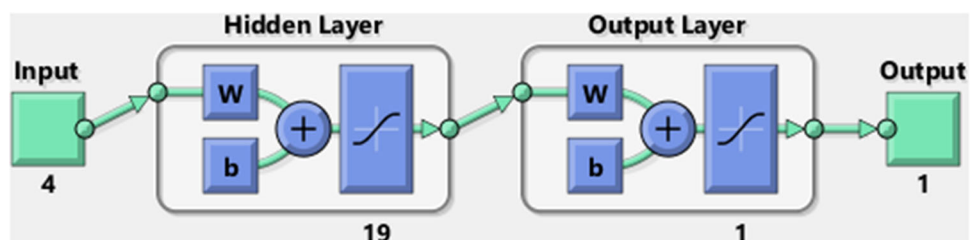
Fig. 8a–c by correlating the experimentally measured data with the ANN predicted data. The figure shows that the predicted response values are in close correlation with their measured values.

5.2 Prediction of μEDM responses by ANFIS

The ANFIS model is integration of ANN learning and fuzzy if–then rule-based decision-making rationale. It develops the mapping relationships among the process response and input data to generate the finest distribution for membership functions. In this section, prognostication of MRR, RLT, and ROC as μEDM output responses by ANFIS is aimed under its operating conditions such as pulse-on time, current, gap voltage, and duty cycle. There are two significant stages in the implementation of the ANFIS model, the creation of pattern vectors is the initial one, while the generation of mapping relationship between the target vectors and their corresponding input condition vectors is the other one. According to the measured experimental data listed in Table 2 for this investigation, out of 33 experimental runs, 24 were randomly selected for training the network, and the rest 9 were selected for testing. In developing the ANFIS model, the input variables of the model such as type and number of MFs and the number of network iterations are essential parameters. However, for a nonlinear process modeling, the appropriate section of these essential parameters is considerably a challenging characteristic. There are no stipulated guidelines or constructive formulations to determine the necessary number of MFs in the literature [47]. Therefore, the number of MFs and their type are determined through the trial-and-error method. Figure 9 shows the derived MFs of the input variables based on trail-error method. The training parameters used for the formulation of the ANFIS predictive model are given in Table 4. Generally, the predictive accuracy of the ANFIS model is evaluated using the root-mean-square error (RMSE). Figure 10a–c shows a good correlation between the developed ANFIS model predicted values based on the selected model training parameters for its formulation and the experimentally measured values for MRR, RLT, and ROC respectively. The results reveal that a good predictive model is constructed based on the employment of appropriate learning and decision-making rationale with the minimum test error to predict the μEDM parameters.
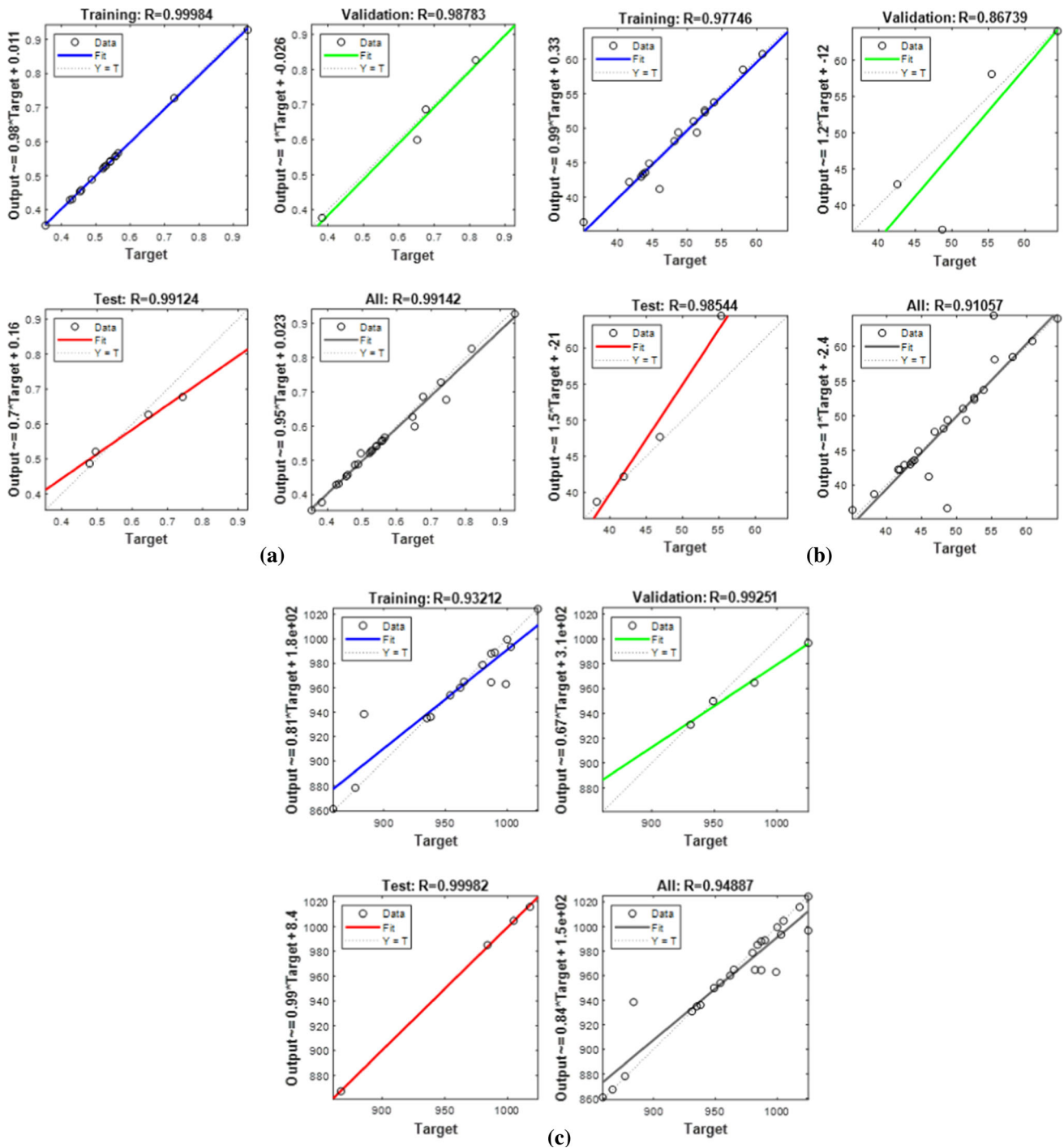
Fig. 6 The determined ANN structure 4-19-1 for μEDM performance characteristics modelling and analysis

Fig. 7 Linear regression analysis between the experimental values and predicted values by FFBP-ANN for training, validation, testing and overall **a** of MRR, **b** of RLT and (**b**) of ROC

5.3 Prediction of μEDM responses by ANFIS trained by GA and ANFIS trained by PSO

Rather than selecting the ANFIS model input parameters randomly, it is proposed their optimal conditions derivation

by the integration of evolutionary based optimization algorithms such as GA and PSO towards the prediction accuracy improvement of the ANFIS model. As evolutionary optimization approaches with their random search, GA and PSO are integrated with ANFIS as the most viable approaches [47]. However, here the appropriate selection of GA and
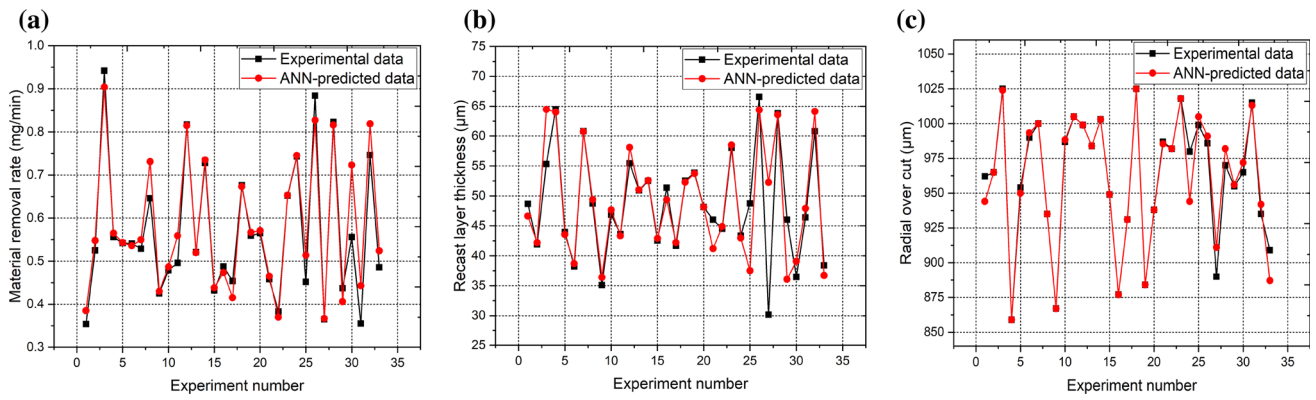
Fig. 8 Comparison of experimental and ANN-predicted data for a) MRR, b) RLT and c) ROC
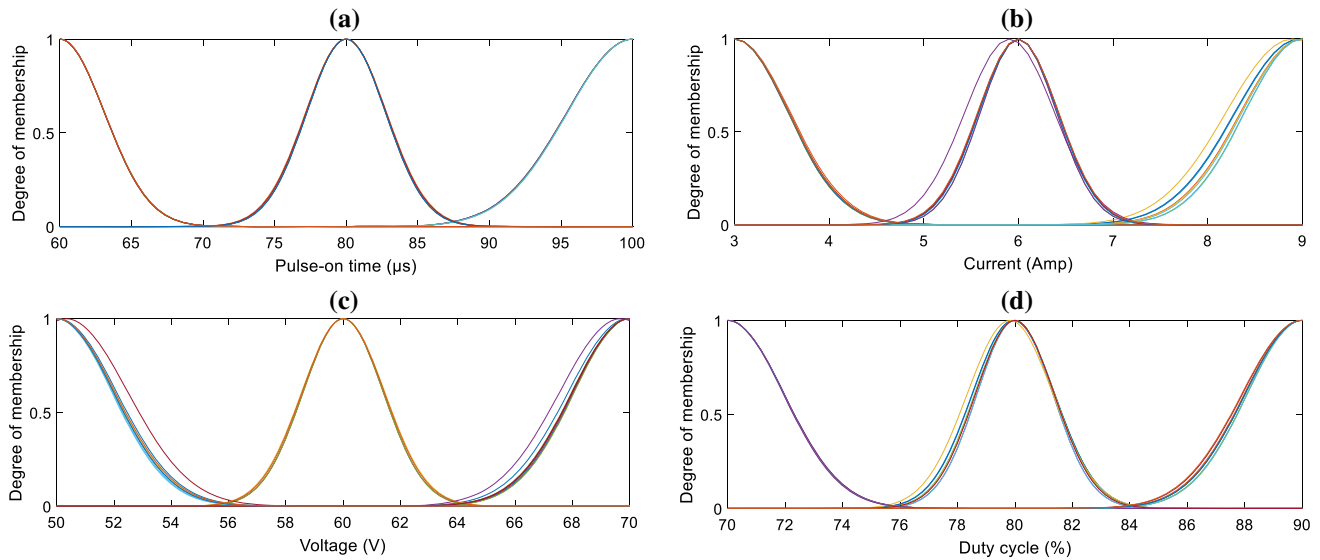
Fig. 9 The MFs for **a** pulse-on time, **b** current, **c** gap voltage, and **d** duty cycle for ANFIS predictive model

Table 4 Training parameters ANFIS predictive models

Parameter	Description/value
Number of nodes	237
Number of linear parameters	115
Total number of parameters	299
Number of training data pairs	24
Number of testing data pairs	9
Number of fuzzy rules	23
Membership function	gaussmf
Optimisation Method	Hybrid (Least square & backpropagation)
Error Tolerance	0.0
Output MF	Linear
Number of model training iterations	2000
Computation time	< 1 min

PSO algorithm-centric parameters intern is another significant task an efficient hybrid ANFIS model development.

The scheme of the ANFIS-GA hybrid algorithm is shown in Fig. 2. Table 5 lists the GA algorithm control parameters used for the simulation of the ANFIS-GA algorithm. The values of GA parameters for this investigation are derived based on the several pilot simulations trials and the identified values are the most appropriate for the present problem. According to the available experimentally measured data listed in Table 2 for this investigation, out of 33 experimental data, 24 were randomly selected for the training of the ANFIS-GA algorithm, and the rest 9 was selected for testing. To establish the ANFIS-GA predictive model, code was generated in MATLAB software. The Gaussian MFs are used for the simulation of the ANFIS-GA algorithm as suggested by many authors. Additionally, in the development of ANFIS-PSO, the number of particles, weight damping inertia ratio, initial inertia weight, the number of iterations, social and cognitive
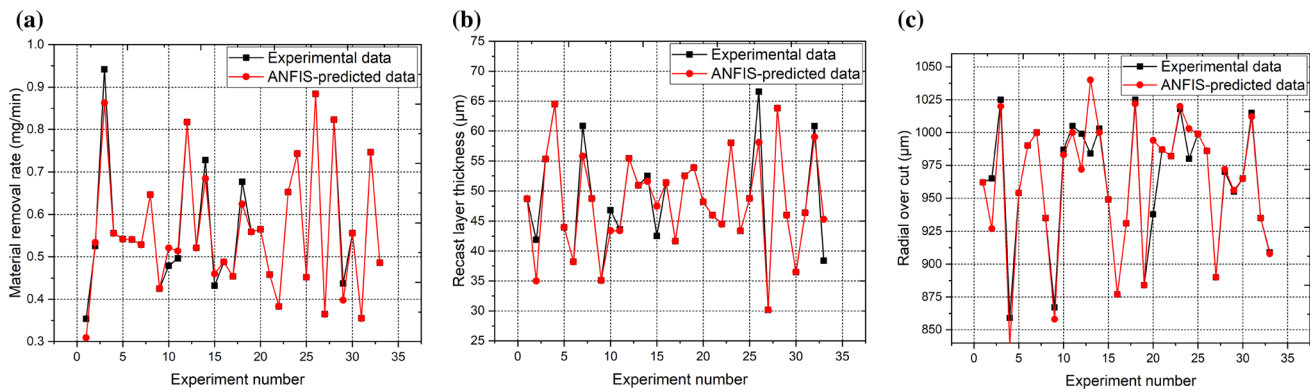
Fig. 10 Comparison of experimental and ANFIS-predicted data for **a** MRR, **b** RLT and **c** ROC

Table 5 GA and PSO algorithm control parameters used for simulation of ANFIS-GA algorithm

GA control parameters for ANFIS-GA algorithm		PSO control parameters for ANFIS-PSO algorithm	
Parameter	Description/Value	Parameter	Description/Value
Population size	35	Max. number of iterations	35
Max. number of generations	2000	Max. number of particles	2000
Mutation percentage	0.8	Initial inertia weight	0.5
Crossover percentage	0.6	Inertia weight damping ratio	0.9
Selection pressure	8	Personal Learning Coefficient	1
Mutation rate	0.1	Global Learning Coefficient	2
Number of fuzzy rules	19	Number of fuzzy rules	19
Computation time	~ 45 min	Computation time	~ 45 min

acceleration are the important parameters of PSO to optimize [41]. To establish the ANFIS-PSO predictive model, code was generated in MATLAB software.

The Gaussian-shaped MFs are considered for this work. According to the available experimentally measured data listed in Table 2 for this investigation, out of 33 experimental data, 24 were randomly selected for the training of the ANFIS-PSO algorithm, and the rest 9 was selected for testing. Table 5 lists the PSO algorithm control parameters used for the simulation of the ANFIS-PSO algorithm. The PSO parameter values were identified as the most appropriate for the present problem and were derived based on several pilot simulation runs and the identified ideal values for PSO parameters such as the number of particles, weight damping inertia ratio, initial inertia weight, the number of iterations, social and cognitive acceleration respectively are 35, 2000, 1, 2, 0.5, and 0.99. The MFs structure corresponding to the ANFIS-GA and ANFIS-PSO are presented in Figs. 11 and 12, respectively. Figure 13a–c and Fig. 14a–c present the

correlation of the hybrid ANFIS models such as ANFIS-GA and ANFIS-PSO predicted data with the experimentally measured data of μEDM responses respectively. A closer correlation between the predicted values and their corresponding experimental values can be observed from these figures.

5.4 Predictability comparison between ANN, ANFIS, ANFIS-GA, and ANFIS-PSO for μEDM responses

Figure 15a, b is the histograms that show the errors distributed in the training and testing data of predicted and experimental values for MRR predictive models of ANN, ANFIS, ANFIS-GA, and ANFIS-PSO. Similarly, Fig. 16a, b and 17a, b are the histograms that show the errors distributed in the training and testing data of predicted and experimental values for RLT and ROC predictive models of ANN, ANFIS, ANFIS-GA, and ANFIS-PSO respectively. The error distribution in these histograms holds the normal distribution.
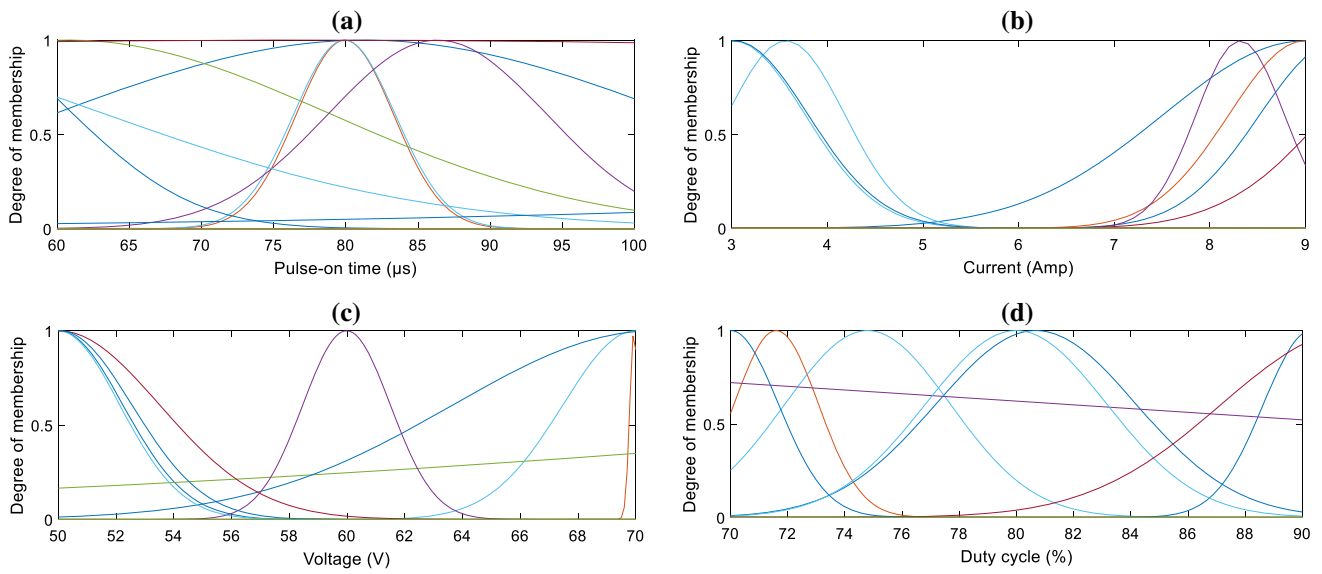
Fig. 11 The MFs for **a** pulse-on time, **b** current, **c** gap voltage, and **d** duty cycle for ANFIS-GA model
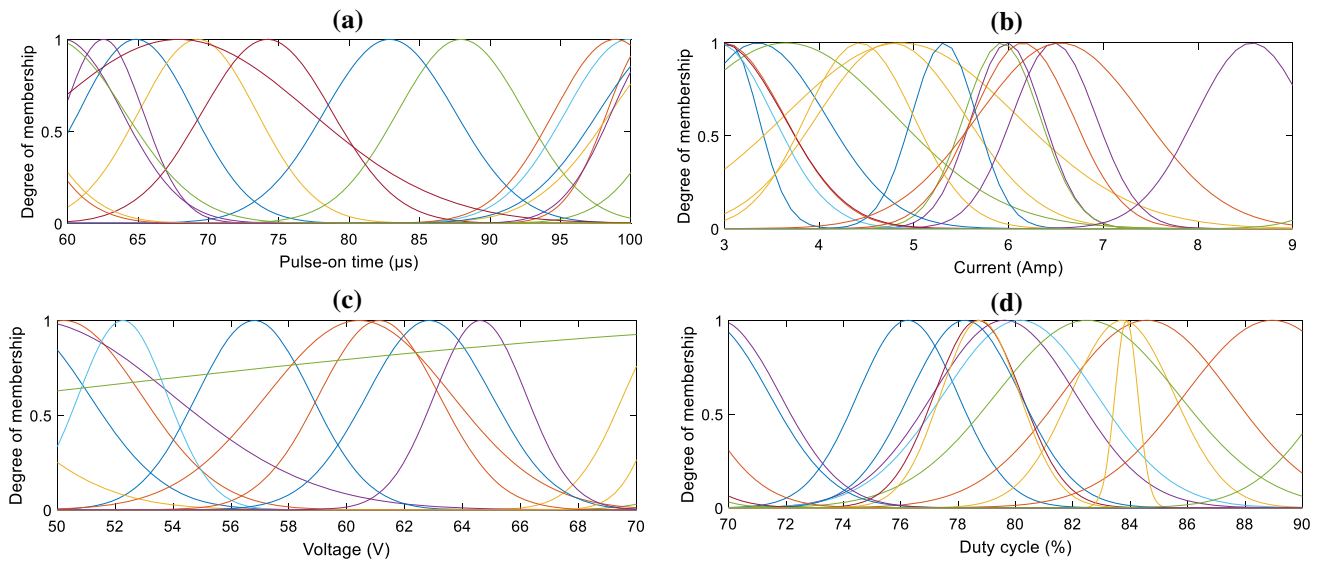

Fig. 12 The MFs for **a** pulse-on time, **b** current, **c** gap voltage, and **d** duty cycle for ANFIS-PSO model
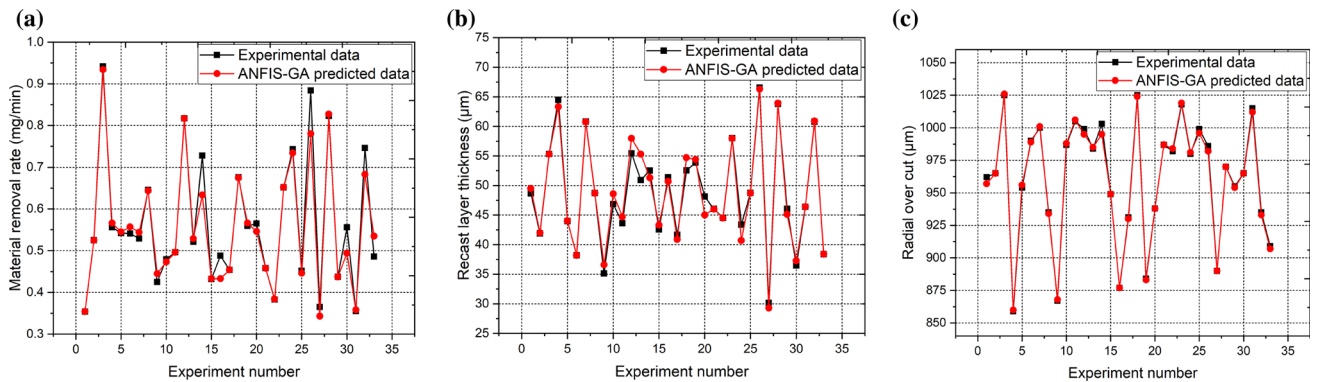

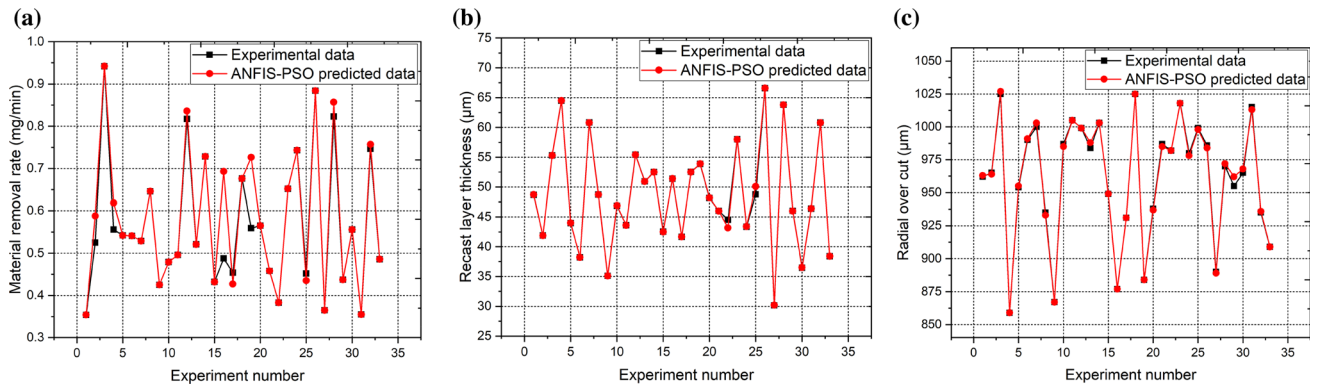**Fig. 13** Comparison of experimental and ANFIS-GA predicted data for **a** MRR, **b** RLT and **c** ROC

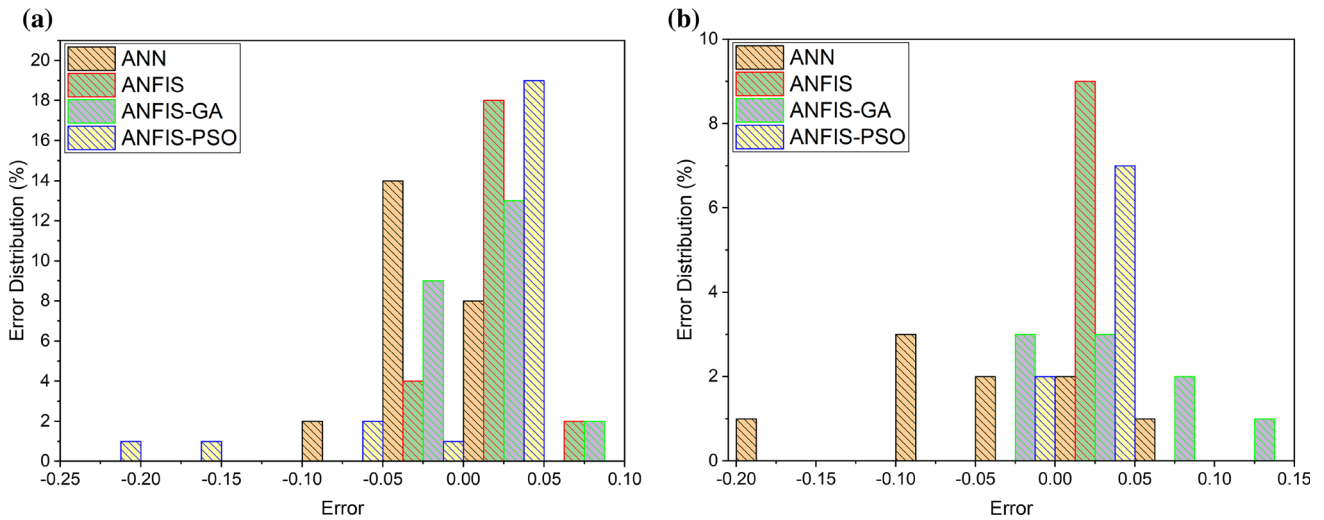**Fig. 14** Comparison of experimental and ANFIS-PSO predicted data for **a** MRR, **b** RLT and **c** ROC

Fig. 15 Histogram of errors for the selectivity of MRR prediction by ANN, ANFIS, ANFIS-GA, and ANFIS-PSO models: **a** training data set and **b** testing data set
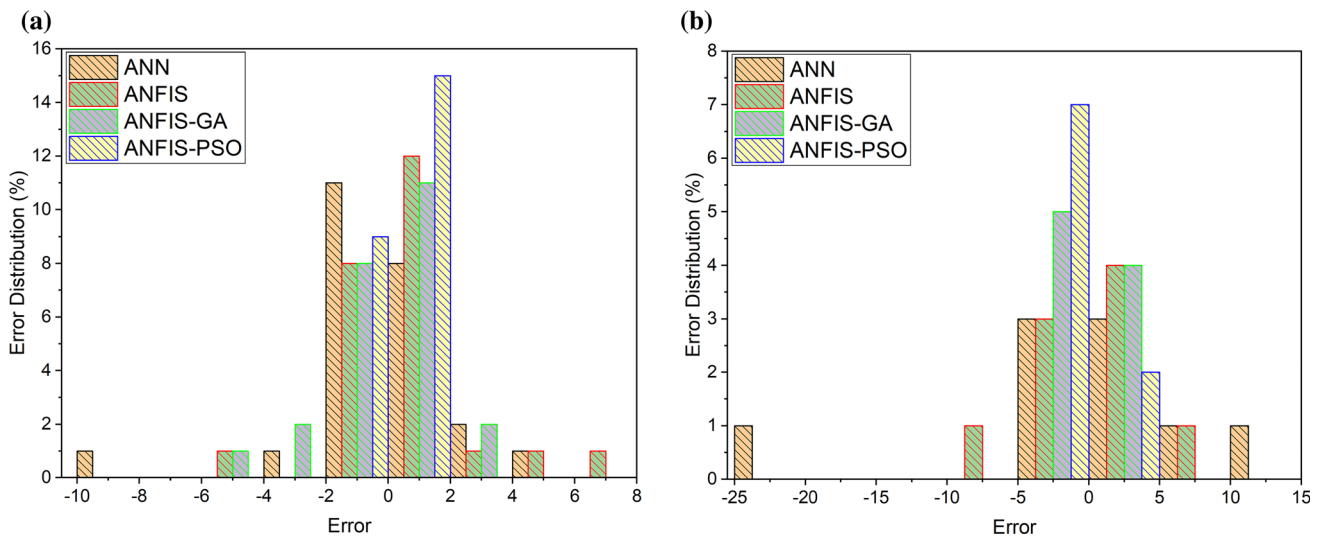

Fig. 16 Histogram of errors for the selectivity of RLT prediction by ANN, ANFIS, ANFIS-GA, and ANFIS-PSO models: **a** training data set and **b** testing data set
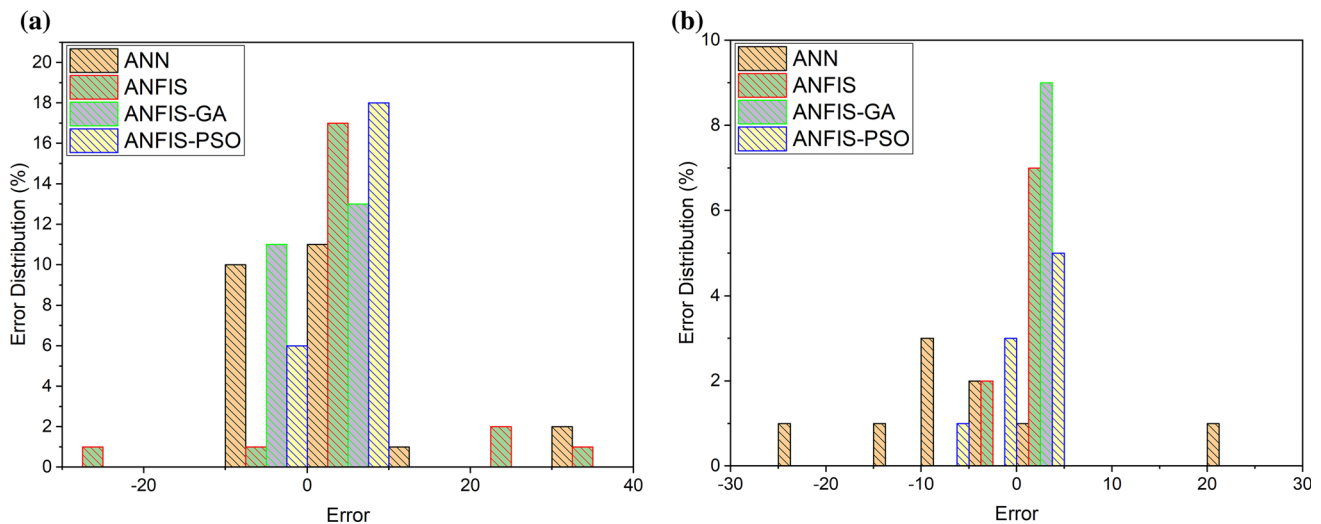
Fig. 17 Histogram of errors for the selectivity of ROC prediction by ANN, ANFIS, ANFIS-GA, and ANFIS-PSO models: **a** training data set and **b** testing data set

The performance of neural network model formulation is generally assessed based on the statistical parameters such as the mean squared relative error (MSRE), root-mean-square error (RMSE), average absolute relative deviation (AARD), and determination coefficient (R^2) evaluated between experimentally measured and the predictive model output data [28, 40]. Computation of these statistical parameters is as follows:

$$MSRE = \frac{1}{N} \sum_N \left(\frac{X_{pred} - X_{exp}}{X_{exp}} \right)^2 \tag{9}$$

$$RSME = \sqrt{\frac{1}{N} \sum_N \left(X_{exp} - X_{pred} \right)^2} \tag{10}$$

$$\% \, AARD = \frac{100}{N} \sum_N \left(\frac{X_{pred} - X_{exp}}{X_{exp}} \right) \tag{11}$$

$$R^2 = 1 - \frac{\sum_{i=1}^{N} \left[X_{pred} - X_{exp} \right]}{\sum_{i=1}^{N} \left[X_{pred} - X_m \right]}, \, X_m = \frac{\sum_{i=1}^{N} \left[X_{pred} \right]}{N} \tag{12}$$

where, X_{pred} is the predictive model output value, X_{exp} is the targeted experimentally measured value, and N is the total number of experimental runs.

The values of MSRE, RMSE and AARD are closer to 0 for the accurate predictive model, whereas the value of R^2 is closer to 1. The calculated values of statistical parameters representing the predictability accuracy of the predictive network models proposed in this work for the prediction of the chosen µEDM responses are listed in Table 6. The values of statistical parameters in Table 6 show that the predicted values by using ANFIS-PSO model are closely correlated to the experimentally measured values of the µEDM responses compared with the predicted values by using ANFIS-GA,

ANFIS, regression, and ANN models. Accordingly, ANFIS-PSO model is recommended as the more suitable algorithm for the prediction of µEDM responses compared with the other models considered in this investigation.

The scatter plots between the data predicted through the developed predictive models and the experimentally measured data are shown in Fig. 18a–c for detailed understanding. The scattered data show a reasonable correlation between the predicted data through all predictive models and experimental data. Considering the three responses, the data scatter of ANFIS-PSO predictive model with experimental data is very less and closer to the line compared to the rest of the predictive models for the training as-well-as testing stage. This explains the precision of the ANFIS-PSO model as superior in comparison with ANFIS-GA, ANFIS, ANN, and regression models for predicting the µEDM performance characteristics.

6 Conclusions

The research work presented the use of a novel hybrid intelligent predictive modeling approach that uses bio-inspired algorithms such as an improved ANFIS with the integration of GA and PSO to predict MRR, RLT, and ROC in the µEDM process. The developed predictive models were assessed statistically to understand their accurate predictability.

The derived conclusions through this investigation are:

1. ANOVA on the experimentally measured date presents the chosen µEDM process control variables are significant for their responses.

Table 6 Performances comparison between the developed predictive models

Response	Model Analysis	Regression	ANN		ANFIS		ANFIS-GA		ANFIS-PSO	
			Training	Testing	Training	Testing	Training	Testing	Training	Testing
MRR	MSRE	0.0009	0.0024	0.0001	0.0019	0.0009	0.0015	0.0053	0.0124	0.0004
	RMSE	0.0155	0.0265	0.0749	0.0257	0.0130	0.0237	0.0490	0.0574	0.0132
	%AARD	0.3860	1.4050	8.0335	0.5934	0.9916	0.6327	3.0336	3.8163	0.2050
	R^2	0.9881	0.9653	0.8815	0.9706	0.9962	0.9716	0.9543	0.8626	0.9972
RLT	MSRE	0.0000	0.0019	0.0721	0.0022	0.0055	0.0010	0.0002	0.0001	0.0001
	RMSE	0.2626	2.2977	9.0770	2.1455	3.6942	1.5719	0.5205	0.2734	0.4532
	%AARD	0.0152	0.4740	4.0512	0.9440	0.2662	0.5103	0.3024	0.1251	0.3359
	R^2	0.9985	0.9128	0.5035	0.9135	0.9196	0.9530	0.9983	0.9986	0.9988
ROC	MSRE	0.0000	0.0001	0.0002	0.0004	0.0001	0.0001	0.0001	0.0001	0.0001
	RMSE	3.2549	10.8264	11.7047	19.9833	1.2910	2.3004	2.1858	1.4434	2.8480
	%AARD	0.0681	7.2181	8.8339	1.8629	0.4183	0.6769	3.2557	0.0649	1.7261
	R^2	0.9956	0.9551	0.9241	0.8606	0.9989	0.9978	0.9950	0.9991	0.9990
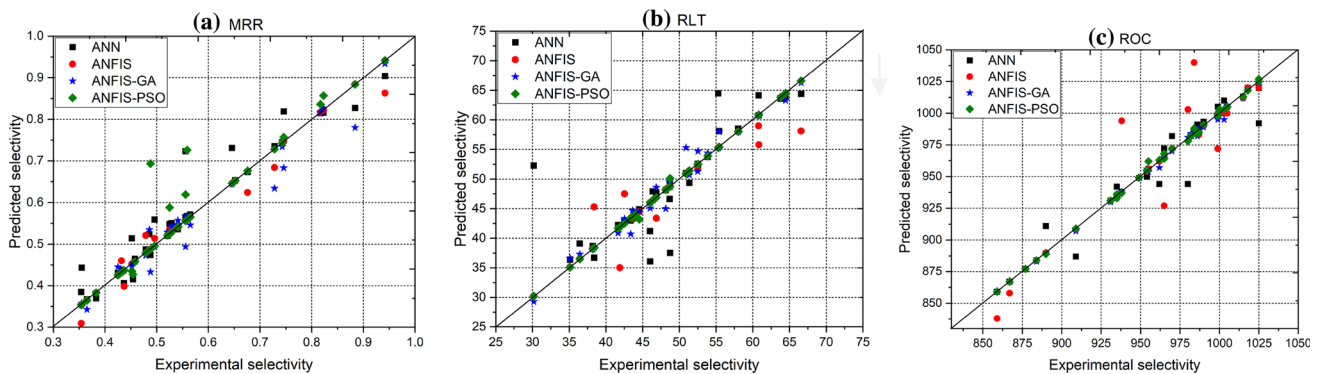
Fig. 18 Comparison of predicted selectivity data against experimental selectivity data for **a** MRR, **b** RLT, and **c** ROC

2. The postulated regression models for MRR, RLT, and ROC can predict their measured value with an accuracy of up to 98.98%, 99.92%, and 99.47% respectively.
3. The predicted training and testing values for the responses with ANN, ANFIS, ANFIS-GA, and ANFIS-PSO were reasonably in good agreement with their corresponding experimentally measured values.
4. Comparison plots of predicted data with ANN, ANFIS, ANFIS-GA, and ANFIS-PSO and experimental values for all the responses are shown with a good correlation.
5. The histograms show the normal distribution of the errors in training and testing data of predicted data with ANN, ANFIS, ANFIS-GA, and ANFIS-PSO and experimental values for all the responses.
6. The estimated MSRE, RMSE, %AARD, and R^2 values of ANFIS-PSO were found to be superior compared with regression, ANFIS-GA, ANFIS, and ANN models.
7. The scatter plots between the data predicted through the developed predictive models and the experimentally measured data also explain the precision of the ANFIS-PSO model as superior in comparison with regression, ANFIS-GA, ANFIS, and ANN models for predicting the μEDM performance characteristics.
8. The computation time noted for the simulation of ANN and ANFIS models was too much lower (less than 1 min) while ANFIS-GA and ANFIS-PSO models were about 45 min.

Declarations

Conflicts of interest The author declares no conflict of interest.

References

1. Frifita, W., Ben Salem, S., Haddad, A., Yallese, M.A.: Optimization of machining parameters in turning of Inconel 718 Nickel-base super alloy. Mech. Ind. **21**(2), 203 (2020). https://doi.org/10.1051/meca/2020001

2. Chandra Behera, B., Sudarsan Ghosh, C., Paruchuri, V.R.: Study of saw-tooth chip in machining of Inconel 718 by metallographic technique. Mach. Sci. Technol. **23**(3), 431–454 (2019). https://doi.org/10.1080/10910344.2019.1575397

3. Hribersek, M., Pusavec, F., Rech, J., Kopac, J.: Modeling of machined surface characteristics in cryogenic orthogonal turning of inconel 718. Mach. Sci. Technol. **22**(5), 829–850 (2018). https://doi.org/10.1080/10910344.2017.1415935

4. Khanna, N., Agrawal, C., Gupta, M.K., Song, Q.: Tool wear and hole quality evaluation in cryogenic drilling of Inconel 718 superalloy. Tribol. Int. **143**, 106084 (2020). https://doi.org/10.1016/j.triboint.2019.106084

5. Jafarian, F.: Electro discharge machining of Inconel 718 alloy and process optimization. Mater. Manuf. Process. **35**(1), 95–103 (2020). https://doi.org/10.1080/10426914.2020.1711919

6. Rao, T.B.: Optimizing machining parameters of wire-EDM process to cut Al7075/SiCp composites using an integrated statistical approach. Adv. Manuf. **4**(3), 202–216 (2016). https://doi.org/10.1007/s40436-016-0148-3

7. Sivaprakasam, P., Hariharan, P., Gowri, S.: Experimental investigations on nano powder mixed micro-wire EDM process of inconel-718 alloy. Meas. J. Int. Meas. Confed. **147**, 106844 (2019). https://doi.org/10.1016/j.measurement.2019.07.072

8. Singh, P., Yadava, V., Narayan, A.: Parametric study of ultrasonic-assisted hole sinking micro-EDM of titanium alloy. Int. J. Adv. Manuf. Technol. **94**(5–8), 2551–2562 (2018). https://doi.org/10.1007/s00170-017-1051-1

9. Tiwary, A.P., Pradhan, B.B., Bhattacharyya, B.: Study on the influence of micro-EDM process parameters during machining of Ti–6Al–4V superalloy. Int. J. Adv. Manuf. Technol. **76**(1–4), 151–160 (2014). https://doi.org/10.1007/s00170-013-5557-x

10. Dilip, D.G., Panda, S., Mathew, J.: Characterization and parametric optimization of micro-hole surfaces in micro-EDM drilling on Inconel 718 superalloy using genetic algorithm. Arab. J. Sci. Eng. (2020). https://doi.org/10.1007/s13369-019-04325-4

11. Pradhan, B.B., Masanta, M., Sarkar, B.R., Bhattacharyya, B.: Investigation of electro-discharge micro-machining of titanium super alloy. Int. J. Adv. Manuf. Technol. **41**(11–12), 1094–1106 (2009). https://doi.org/10.1007/s00170-008-1561-y

12. Jahan, M.P., Wong, Y.S., Rahman, M.: Experimental investigations into the influence of major operating parameters during micro-electro discharge drilling of cemented carbide. Mach. Sci. Technol. **16**(1), 131–156 (2012). https://doi.org/10.1080/10910344.2012.648575

13. J. Cyril Pilligrin, P. Asokan, J. Jerald, G. Kanagaraj, J. Mukund Nilakantan, and I. Nielsen, "Tool speed and polarity effects in micro-EDM drilling of 316L stainless steel," *Prod. Manuf. Res.*, vol. 5, no. 1, pp. 99–117, 2017, doi: https://doi.org/10.1080/21693277.2017.1357055.

14. Jabbaripour, B., Sadeghi, M.H., Faridvand, S., Shabgard, M.R.: Investigating the effects of EDM parameters on surface integrity, MRR and TWR in machining of Ti–6Al–4V. Mach. Sci. Technol. **16**(3), 419–444 (2012). https://doi.org/10.1080/10910344.2012.698971

15. Liu, Q., Zhang, Q., Zhu, G., Wang, K., Zhang, J., Dong, C.: Effect of electrode size on the performances of micro-EDM. Mater. Manuf. Process. **31**(4), 391–396 (2016). https://doi.org/10.1080/10426914.2015.1059448

16. Tsai, Y.Y., Masuzawa, T.: An index to evaluate the wear resistance of the electrode in micro-EDM. J. Mater. Process. Technol. **149**(1–3), 304–309 (2004). https://doi.org/10.1016/j.jmatprotec.2004.02.043

17. Lim, H.S., Wong, Y.S., Rahman, M., Edwin Lee, M.K.: A study on the machining of high-aspect ratio micro-structures using micro-EDM. J. Mater. Process. Technol. **140**(1–3), 318–325 (2003). https://doi.org/10.1016/S0924-0136(03)00760-X

18. Ay, M., Çaydaş, U., Hasçalik, A.: Optimization of micro-EDM drilling of Inconel 718 superalloy. Int. J. Adv. Manuf. Technol. **66**(5–8), 1015–1023 (2013). https://doi.org/10.1007/s00170-012-4385-8

19. Bamberg, E., Heamawatanachai, S.: Orbital electrode actuation to improve efficiency of drilling micro-holes by micro-EDM. J. Mater. Process. Technol. **209**(4), 1826–1834 (2009). https://doi.org/10.1016/j.jmatprotec.2008.04.044

20. Natarajan, N., Suresh, P.: Experimental investigations on the micro-hole machining of 304 stainless steel by micro-EDM process using RC-type pulse generator. Int. J. Adv. Manuf. Technol. **77**(9–12), 1741–1750 (2015). https://doi.org/10.1007/s00170-014-6494-z

21. Rao, T.B., Reddy, K.D.K., Srikar, K.B., Krishna, M.P., Kumar, C.P.: Simultaneous optimization of M-EDM parameters for machining Inconel 718 super alloy. Int. J. Mech. Eng. Technol. **9**(5), 436–444 (2018)

22. Somashekhar, K.P., Ramachandran, N., Mathew, J.: Optimization of material removal rate in micro-EDM using artificial neural network and genetic algorithms. Mater. Manuf. Process. **25**(6), 467–475 (2010). https://doi.org/10.1080/10426910903365760

23. Surleraux, A., Lepert, R., Pernot, J.-P., Kerfriden, P., Bigot, S.: Machine Learning based reverse modelling approach for rapid tool shape optimization in die-sinking μEDM. J. Comput. Inf. Sci. Eng. **20**(June), 1–25 (2020). https://doi.org/10.1115/1.4045956

24. Suganthi, X.H., Natarajan, U., Sathiyamurthy, S., Chidambaram, K.: Prediction of quality responses in micro-EDM process using an adaptive neuro-fuzzy inference system (ANFIS) model. Int. J. Adv. Manuf. Technol. **68**(1–4), 339–347 (2013). https://doi.org/10.1007/s00170-013-4731-5

25. Sharma, D., Bhowmick, A., Goyal, A.: Enhancing EDM performance characteristics of Inconel 625 superalloy using response surface methodology and ANFIS integrated approach. CIRP J. Manuf. Sci. Technol. **37**, 155–173 (2022). https://doi.org/10.1016/j.cirpj.2022.01.005

26. Goyal, A., Sharma, D., Bhowmick, A., Pathak, V.K.: Experimental investigation for minimizing circularity and surface roughness under nano graphene mixed dielectric EDM exercising fuzzy-ANFIS approach. Int. J. Interact. Des. Manuf. **16**(3), 1135–1154 (2022). https://doi.org/10.1007/s12008-021-00826-5

27. Singh, J.: Multi-objective optimization of powder-mixed EDM parameters using hybrid Grey-ANFIS artificial intelligence technique. Int. J. Interact. Des. Manuf. (2022). https://doi.org/10.1007/s12008-022-00866-5

28. Singh, N.K., Singh, Y., Kumar, S., Upadhyay, R.: Integration of GA and neuro-fuzzy approaches for the predictive analysis of gas-assisted EDM responses. SN Appl. Sci. **2**(1), 1–14 (2020). https://doi.org/10.1007/s42452-019-1533-x

29. Bhiradi, I., Raju, L., Hiremath, S.S.: Adaptive neuro-fuzzy inference system (ANFIS): modelling, analysis, and optimisation of process parameters in the micro-EDM process. Adv. Mater. Process. Technol. **6**(1), 133–145 (2020). https://doi.org/10.1080/2374068X.2019.1709309

30. Zhang, L., Jia, Z., Wang, F., Liu, W.: A hybrid model using supporting vector machine and multi-objective genetic algorithm for processing parameters optimization in micro-EDM. Int. J. Adv. Manuf. Technol. **51**(5–8), 575–586 (2010). https://doi.org/10.1007/s00170-010-2623-5

31. Assarzadeh, S., Ghoreishi, M.: Neural-network-based modeling and optimization of the electro-discharge machining process. Int. J. Adv. Manuf. Technol. **39**(5–6), 488–500 (2008). https://doi.org/10.1007/s00170-007-1235-1

32. Fazlollahtabar, H., Gholizadeh, H.: Fuzzy possibility regression integrated with fuzzy adaptive neural network for predicting and optimizing electrical discharge machining parameters. Comput. Ind. Eng. **140**, 106225 (2020). https://doi.org/10.1016/j.cie.2019.106225

33. Saffaran, A., Azadi Moghaddam, M., Kolahan, F.: Optimization of backpropagation neural network-based models in EDM process using particle swarm optimization and simulated annealing algorithms. J. Braz. Soc. Mech. Sci. Eng. **42**(1), 1–14 (2020). https://doi.org/10.1007/s40430-019-2149-1

34. Jang, J.S.R.: ANFIS: adaptive-network-based fuzzy inference system. IEEE Trans. Syst. Man Cybern. **23**(3), 665–685 (1993). https://doi.org/10.1109/21.256541

35. Kumar, S., Dhanabalan, S., Narayanan, C.S.: Application of ANFIS and GRA for multi-objective optimization of optimal wire-EDM parameters while machining Ti–6Al–4V alloy. SN Appl. Sci. **1**(4), 1–12 (2019). https://doi.org/10.1007/s42452-019-0195-z

36. Maher, I., Eltaib, M.E.H., Sarhan, A.A.D., El-Zahry, R.M.: Cutting force-based adaptive neuro-fuzzy approach for accurate surface roughness prediction in end milling operation for intelligent machining. Int. J. Adv. Manuf. Technol. **76**(5–8), 1459–1467 (2014). https://doi.org/10.1007/s00170-014-6379-1

37. Aydin, M., Karakuzu, C., Uçar, M., Cengiz, A., Çavuşlu, M.A.: Prediction of surface roughness and cutting zone temperature in dry turning processes of AISI304 stainless steel using ANFIS with PSO learning. Int. J. Adv. Manuf. Technol. **67**(1–4), 957–967 (2013). https://doi.org/10.1007/s00170-012-4540-2

38. Demircan, C., Bayrakçı, H.C., Keçebaş, A.: Machine learning-based improvement of empiric models for an accurate estimating process of global solar radiation. Sustain. Energy Technol. Assess. **37**(June), 2020 (2019). https://doi.org/10.1016/j.seta.2019.100574

39. Moayedi, H., Raftari, M., Sharifi, A., Jusoh, W.A.W., Rashid, A.S.A.: Optimization of ANFIS with GA and PSO estimating α ratio in driven piles. Eng. Comput. **36**(1), 227–238 (2020). https://doi.org/10.1007/s00366-018-00694-w

40. Rezakazemi, M., Dashti, A., Asghari, M., Shirazian, S.: H2-selective mixed matrix membranes modeling using ANFIS, PSO-ANFIS, GA-ANFIS. Int. J. Hydrog. Energy **42**(22), 15211–15225 (2017). https://doi.org/10.1016/j.ijhydene.2017.04.044

41. Xu, L., Huang, C., Li, C., Wang, J., Liu, H., Wang, X.: Estimation of tool wear and optimization of cutting parameters based on novel ANFIS-PSO method toward intelligent machining. J. Intell. Manuf. (2020). https://doi.org/10.1007/s10845-020-01559-0

42. Rao, T.B., Krishna, A.G., Katta, R.K., Krishna, K.R.: Modeling and multi-response optimization of machining performance while turning hardened steel with self-propelled rotary tool. Adv. Manuf. **3**(1), 84–95 (2015). https://doi.org/10.1007/s40436-014-0092-z

43. Srivastava, A., Dubey, A.K., Shrivastava, P.K.: Computer-aided hybrid ANN-GA approach for modelling and optimisation of EDDG process. Int. J. Abras. Technol. **5**(3), 245–257 (2012). https://doi.org/10.1504/IJAT.2012.051034

44. Mathai, V.J., Dave, H.K., Desai, K.P.: End wear compensation during planetary EDM of Ti–6Al–4V by adaptive neuro fuzzy inference system. Prod. Eng. (2018). https://doi.org/10.1007/s11740-017-0778-8

45. Lin, H.L.: Optimization of Inconel 718 alloy welds in an activated GTA welding via Taguchi method, gray relational analysis, and a neural network. Int. J. Adv. Manuf. Technol. **67**(1–4), 939–950 (2013). https://doi.org/10.1007/s00170-012-4538-9

46. Prabhu, S., Uma, M., Vinayagam, B.K.: Adaptive neuro-fuzzy interference system modelling of carbon nanotube-based electrical discharge machining process. J. Braz. Soc. Mech. Sci. Eng. **35**(4), 505–516 (2013). https://doi.org/10.1007/s40430-013-0047-5

47. Diani, J., Gall, K.: Finite strain 3D thermoviscoelastic constitutive model. Society (2006). https://doi.org/10.1002/pen